arXiv:1402.5450v1 [cs.RO] 21 Feb 2014

State Estimation for a Humanoid Robot

Nicholas Rotella, Michael Bloesch, Ludovic Righetti and Stefan Schaal

***Abstract*— This paper introduces a framework for state estimation on a humanoid robot platform using only common proprioceptive sensors and knowledge of leg kinematics. The presented approach extends that detailed in [1] on a quadruped platform by incorporating the rotational constraints imposed by the humanoid's flat feet. As in previous work, the proposed Extended Kalman Filter (EKF) accommodates contact switching and makes no assumptions about gait or terrain, making it applicable on any humanoid platform for use in any task. The filter employs a sensor-based prediction model which uses inertial data from an IMU and corrects for integrated error using a kinematics-based measurement model which relies on joint encoders and a kinematic model to determine the relative position and orientation of the feet. A nonlinear observability analysis is performed on both the original and updated filters and it is concluded that the new filter significantly simplifies singular cases and improves the observability characteristics of the system. Results on simulated walking and squatting datasets demonstrate the performance gain of the flat-foot filter as well as confirm the results of the presented observability analysis.**

I. INTRODUCTION

State estimation has long been a topic of importance in mobile robotics, where the typical filter architecture fuses wheel odometry (also known as "dead reckoning") with exteroceptive sensors in order to correct for errors due to wheel slippage and other factors. In most cases, state estimation entails maintaining an accurate estimate of the robot's absolute position and yaw as these are sufficient for navigation in simple environments.

Unlike traditional mobile robot platforms, however, legged robots usually require knowledge of the full 6DOF pose of the base for control. Further, the utility of such platforms is their potential for operation in unstructured environments. Exteroceptive sensors such as cameras or GPS units are unfit for use in such situations, forcing the tasks of control and localization to depend on proprioceptive sensing. While wheeled robots are assumed to remain stable and in contact at all times, legged robot locomotion inherently involves intermittent contacts. This makes stability a main concern as well as complicates odometry-based estimation approaches. The problem of state estimation for legged robots is thus fundamentally different than that of estimation for wheeled robots. The goal of this work is thus to develop a state estimation framework suitable for the task of bipedal legged locomotion. As such, it is useful to review traditional approaches in order to better define the goals of this work.

At its simplest, legged state estimation entails determination of the homogeneous transformation which describes the robot's pose relative to an initial pose. One of the earliest attempts [2] was performed on the CMU Ambler, a hexapod robot having only joint encoders. The positions of the feet were computed both from motor commands and from encoder measurements. Each foot contributed a measurement and the transformation which minimized the squared error between the two estimates was computed.

Nearly fifteen years later, the approach detailed by Gassmann et al. in [3] relied on the same dead-reckoning method, extending earlier work by fusing odometry with orientation and position measurements from newly-available inertial sensors such as MEMS IMU and GPS units. However, this approach was inherently unable to handle non statically-stable gaits.

Around the same time, Lin et al. [4] extended previous work on pose estimation using a strain-based model with MEMS inertial sensors to measure motion of the body. The gait was split into multiple phases, each of which corresponded to a simple Kalman filter. Models for each phase were switched in and out using sensory cues, allowing non statically-stable gaits. However, it was shown that the filter provides accurate pose estimates only when in tripod support.

Chitta et al. employed a particle filter which used an odometry-based prediction model for the COM during quadruple support and an update model based on IMU data, joint encoder readings and knowledge of the terrain relief for state estimation with the quadruped LittleDog in [5]. While this method permitted global localization, it assumed knowledge of the terrain and a statically-stable gait.

Cobano et al. introduced a state estimator in [6] for the quadruped SILO4 which fused changes in position (computed using dead-reckoning) with magnetometer and DGPS measurements in an Extended Kalman Filter. While they tracked global position and heading without gait assumptions, their approach was limited in that the full 6DOF pose was not estimated.

In [7], Reinstein and Hoffmann introduced an EKF for their quadruped which combined kinematic predictions from IMU data with a "data-driven" velocity measurement. By assuming an uninterrupted gait, the velocity was computed using a learned model. However, the gait assumption limits the utility of their approach. Further, the data-driven model used for corrections was very specific to their platform.

Recent work [8] on the DLR Crawler hexapod platform

N. Rotella is with the Computational Learning and Motor Control Lab, University of Southern California, Los Angeles, California. Email: nrotella@usc.edu

M. Bloesch is with the Autonomous Systems Lab, ETH Zurich, Zurich, Switzerland. Email: bloeschm@ethz.ch

L. Righetti and S. Schaal are with the Autonomous Motion Department, Max Planck Institute for Intelligent Systems, Tuebingen, Germany. Email: ludovic.righetti@tuebingen.mpg.de,sschaal@mpi-is.de

by Chilian et al. introduced an information filter suitable for combining multiple types of measurements. The process model integrated IMU data to track the pose of the hexapod while visual and leg odometry were used for updates. Absolute measurements of roll and pitch angles were obtained from the accelerometer and used as well. While they made no gait assumptions, their leg odometry measurements were valid only during periods of three or more contacts. In addition, the other sensors used are unreliable in complex environments.

Biped state estimation has only recently gained attention. Park et al. [9] introduced a Kalman Filter in the context of a ZMP balance controller using the Linear Inverted Pendulum Model (LIPM) to approximate the dynamics of the humanoid robot. The position, velocity, and acceleration of the COM of the LIPM were estimated using the pendulum dynamics and the measured ZMP location was used for the update step. However, their approach was only applicable in the context of ZMP balancing and walking and so its impact was limited.

In a similar context, Wang et al. proposed in [10] an Unscented Kalman Filter which provided estimates of the joint angles and velocities for predictive ZMP control. The filter treated the biped in single support as a fixed-base manipulator with corresponding dynamics. Of course, this assumption was violated if the robot lost contact or slipped. Additionally the absolute orientation relative to gravity could not be predicted. This filter was also computationally-demanding as it used the full manipulator dynamics at every timestep for prediction.

Given the above assessment of previous work, it is conjectured that a suitable filter for general biped state estimation should 1) use only proprioceptive sensors 2) make no assumptions about the gait or terrain 3) be easily adapted to any humanoid platform and 4) use as little computational resources as possible. In [1], Bloesch et al. introduced a novel Extended Kalman Filter for state estimation on the quadruped starlETH which fused leg odometry and IMU data to estimate the full pose of the robot without making these assumptions. Further, it was shown that as long as one foot is in contact with the ground then all states other than absolute position and heading (neither of which matters for stability) are observable. Combined with the fact that contact switching can easily be handled, this result makes the filter applicable to bipeds which experience intermittent contacts and even transient aerial phases. The goal of this work is to adapt this approach to a humanoid platform by incorporating into the filter the rotational constraints provided by the flat feet of the biped; intuitively, a single flat foot contact fully constrains the pose of the robot. This suggests superior performance of the augmented filter in the single contact phase which is crucial for walking. In addition, the new estimates of foot orientations can be used for controlling contacts. This extension is shown through theoretical analysis to improve the observability properties of the filter and to increase the accuracy of the estimation as demonstrated on simulated walking data having realistic noise levels. We proceed in the following sections by reviewing the state estimation framework as introduced in [1].

II. Estimation Framework

In order to introduce required terminology and notation, we begin by briefly reviewing the problem of state estimation for linear and nonlinear systems.

The Kalman Filter provides an estimate of the state vector x equal to the expected value of the state given all prior measurements along with a corresponding covariance matrix P which specifies the uncertainty of the estimate. The filter involves 1) propagating the expected value and estimation error covariance of the state through the system in the *prediction* step to produce the *a priori* estimates $\hat{x}_k^-$ and P_k^- and 2) updating the expected value and covariance of the state using a measurement in the *update step* to produce the *a posteriori* estimates $\hat{x}_k^+$ and P_k^+.

However, the standard Kalman Filter is applicable only for state estimation in linear systems. Suppose we have the continuous-time, nonlinear system

$$\dot{x} = f(x, w) \tag{1}$$

$$y = h(x, v) \tag{2}$$

where the nonlinear function $f()$ is the *process* or *prediction* model and the nonlinear function $h()$ is the *measurement* or *update* model. One of the simplest ways to perform state estimation for this nonlinear system is to linearize the models around the current estimate at each timestep and apply the Kalman Filter equations. This is known as the *Extended Kalman Filter* or the *error state* Kalman Filter. While the optimality and convergence of the filter are no longer guaranteed, this approach has become one of the most commonly-used tools in nonlinear state estimation. We chose the EKF over alternatives such as the Particle Filter (PF) or Unscented Kalman Filter (UKF) primarily for its simplicity and low computational costs. However, the general estimation framework and subsequent observability analysis presented in this work are applicable to any of these filters.

The EKF algorithm works as follows. First, (1) and (2) are discretized and the *a priori* state and measurement are computed using the resulting discretized models as follows.

$$\hat{x}_k^- = f(\hat{x}_{k-1}^+) \tag{3}$$

$$\hat{y}_k = h(\hat{x}_k^-) \tag{4}$$

Next, the process and measurement models (1) and (2) are linearized around the *a priori* state estimate using a first-order Taylor series expansion to produce the process and measurement Jacobians F_k and H_k. The prediction step is completed by computing the *a priori* covariance using the linearized prediction model.

$$F_k = \frac{\partial f}{\partial x}|_{\hat{x}_k^-} \tag{5}$$

$$H_k = \frac{\partial h}{\partial x}|_{\hat{x}_k^-} \tag{6}$$

$$P_k^- = F_k P_{k-1}^+ F_k^T + Q_k \tag{7}$$

where Q_k is the discrete process noise covariance. Finally, when a measurement y_k becomes available the state and covariance matrix are updated using the linearized model as follows.

$$S_k = H_k P_k^- H_k^T + R_k \tag{8}$$
$$K_k = P_k^- H_k^T S_k^{-1} \tag{9}$$
$$\hat{x}_k^+ = \hat{x}_k^- + K_k(y_k - \hat{y}_k) \tag{10}$$
$$P_k^+ = (I - K_k H_k) P_k^- \tag{11}$$

where R_k is the discrete measurement noise covariance. The filter is initialized with an estimate $\hat{x}_0^+$ of the state and corresponding covariance matrix P_0^+ which represents the uncertainty in the chosen initial state.

III. Handling of Rotational Quantities

The unit quaternion was chosen to represent the base orientation in the original filter due to its theoretical and computational advantages. However, since the quaternion is a non-minimal representation of $SO(3)$, special care must be taken in handling rotational quantities in the EKF.

First, the exponential map

$$\exp(\omega) = \begin{pmatrix} \sin(\frac{||\omega||}{2})\frac{\omega}{||\omega||} \\ \cos(\frac{||\omega||}{2}) \end{pmatrix} \tag{12}$$

is used to relate a quaternion at times k and $k+1$ given an incremental rotation of magnitude $||\omega||$ about the unit vector $\omega/||\omega||$. That is,

$$q_{k+1} = \exp(\omega) \otimes q_k \tag{13}$$

where $\otimes$ denotes quaternion multiplication. Roughly speaking, the exponential map is used for "addition" of rotational quantities. Note that the first entry of (12) is the vector portion of the quaternion while the second entry is the scalar portion. This is the convention we employ in this work.

In the EKF state vector, a quaternion state is represented by its corresponding three-dimensional *error rotation vector* ϕ. The covariance of the orientation represented by the quaternion is thus defined with respect to this minimal representation.

During the update step, the innovations vector e corresponding to a quaternion-valued measurement is computed as the three dimensional rotation vector extracted from the difference between the actual measurement quaternion s and the expected measurement quaternion z. That is,

$$e = \log(s \otimes z^{-1}) \tag{14}$$

where $\log()$ denotes the logarithm mapping an element of $SO(3)$ to its corresponding element of $so(3)$ (the inverse of the exponential map). The above operation extends the notion of subtraction to rotational quantities.

Finally, using the innovations vector as computed above, the state correction vector Δx is computed during the update step as $\Delta x = Ke$. While all non-rotational states are updated simply as $\hat{x}_k^+ = \hat{x}_k^- + \Delta x$, a quaternion state is updated using (12) as follows.

$$\hat{q}_k^+ = \exp(\Delta\phi) \otimes \hat{q}_k^- \tag{15}$$

For more information on quaternions and their use in state estimation see [11].

IV. Biped Prediction and Measurement Models

In [1], a continuous-time, nonlinear prediction model describing the time evolution of the state of the quadruped was developed based on rigid body kinematics and a simple model of an IMU consisting of a three-axis accelerometer and a three-axis gyroscope. This prediction model is shown below. Note that this formulation can accommodate an arbitrary number of feet, denoted N.

$$\dot{r} = v \tag{16}$$
$$\dot{v} = a = C^T(\tilde{f} - b_f - w_f) + g \tag{17}$$
$$\dot{q} = \frac{1}{2}\begin{bmatrix} \tilde{\omega} - b_\omega - w_\omega \\ 0 \end{bmatrix} \otimes q \tag{18}$$
$$\dot{p}_i = C^T w_{p,i} \quad \forall i \in \{1, \ldots, N\} \tag{19}$$
$$\dot{b}_f = w_{bf} \tag{20}$$
$$\dot{b}_\omega = w_{b\omega} \tag{21}$$

The state of the filter is $x = [r, v, q, p_i, b_f, b_w]$ where r is the position of the IMU (assumed to be located at the base of the robot), v is the base velocity, q is the quaternion representing a rotation from the world frame to the body frame, p_i is the position of the i^{th} foot in the world frame and b_f and b_w are the gyroscope and accelerometer bias vectors, respectively. Unless otherwise noted, C is used to represent the rotation matrix corresponding to the base pose q. The raw accelerometer and gyroscope measurements are denoted $\tilde{f}$ and $\tilde{\omega}$ and are modeled as being subject to additive thermal noise processes denoted w_f and w_ω as well as random-walk biases parameterized by the noise processes w_{bf} and $w_{b\omega}$. Finally, $w_{p,i}$ denotes the noise process representing the uncertainty of the position of the i^{th} foothold. For more details on the prediction model of the filter, see [1].

In order to extend the established filter to a humanoid platform, we now augment state vector with the quaternions representing the orientations of the feet. Including only one foot in the filter equations for brevity, the new state is thus defined as $x = [r, v, q, p, b_f, b_w, z]$ where z is the quaternion representing the rotation from the world frame to the foot frame. Analogous to the assumption made in [1] about the foot position, it is here assumed that the orientation of the foot remains constant while it is in contact with the ground. In order to permit a small amount of rotational slippage, the corresponding prediction equation is defined to be

$$\dot{z} = \frac{1}{2}\begin{bmatrix} w_z \\ 0 \end{bmatrix} \otimes z \tag{22}$$

where w_z is the process noise term having covariance matrix Q_z. The foot orientation noise is treated as an angular velocity and formed into a *pure* quaternion (zero scalar part) order to remain consistent with the original model. For details about the definition of the derivative of a quaternion derivative, again see [11].

The original filter update step was performed using one measurement equation for each foot which represented the position of that foot relative to the base as measured in the base frame. This measurement is a function only of the measured joint angles and the kinematic model of the leg. The measurement model which relates the measurements to the state vector is thus

$$s_p = C(p - r) + n_p \tag{23}$$

The noise vector n_p represents the combination of noise in the encoder measurements plus uncertainty in the kinematic model. Its covariance is one of the main tuning parameters of the filter.

Following the original filter formulation, we introduce an additional measurement which is again a function of only the measured joint angles and the kinematics model. The orientation of the foot in the base frame represented by the quaternion

$$s_z = \exp(n_q) \otimes q \otimes z^{-1} \tag{24}$$

makes use of the rotational constraint imposed by a flat foot contact in order to provide information about the orientations of the base and foot. The noise term n_q is applied using the exponential map as detailed in the previous section. As with the noise on the relative foot position measurement, this noise term is a function of the uncertainties in the encoders and in the kinematic model and thus constitutes a tuning parameter.

Note all measurements are valid only when the corresponding foot is in contact with the ground without slipping. When a foot is no longer in contact, its pose is temporarily dropped from the filter. In practice, this can be achieved more simply by setting the variances of w_p and w_z corresponding to the foot to large values. The foot's measurement equations are also dropped from the update. This causes the uncertainty corresponding to these states to grow rapidly. When contact is restored, the measurements for that foot are included and the variances are set to their nominal values, triggering a reset of the foot pose to its new value due to the buildup in uncertainty. This allows for handling of intermittent contacts without the need for separate models. During an aerial phase, all measurements and foot states are dropped and the filter reduces to integration of the prediction model.

V. Implementation Details

Since the above system is continuous and nonlinear, it must be discretized and linearized for implementation purposes. Following the EKF framework outlined above, this requires two systems of equations: a *discrete, nonlinear* system for prediction of the state and measurement and a *discrete, linear* system for propagation of the state covariance through the prediction model and for computation of the gain in the update step. Additionally, we will derive in an intermediate step a continuous, linear system. We begin with a discussion of the discrete, nonlinear system used for prediction.

A. Discrete, Nonlinear Model

The first step in the EKF is the propagation of the expected value of the state using the discretized nonlinear model as in (3). Assuming a zero-order hold on the IMU data over a small timestep Δt, we may discretize the original system using a first-order integration scheme as

$$\hat{r}^-_{k+1} = \hat{r}^+_k + \Delta t \hat{v}^+_k + \frac{\Delta t^2}{2}(\hat{C}^{+T}_k \hat{f}_k + g) \tag{25}$$

$$\hat{v}^-_{k+1} = \hat{v}^+_k + \Delta t(\hat{C}^{+T}_k \hat{f}_k + g) \tag{26}$$

$$\hat{q}^-_{k+1} = \exp(\Delta t \hat{\omega}_k) \otimes \hat{q}^+_k \tag{27}$$

$$\hat{p}^-_{i,k+1} = \hat{p}^+_{i,k} \quad \forall i \in \{1, \ldots, N\} \tag{28}$$

$$\hat{b}^-_{f,k+1} = \hat{b}^+_{f,k} \tag{29}$$

$$\hat{b}^-_{\omega,k+1} = \hat{b}^+_{\omega,k} \tag{30}$$

$$\hat{z}^-_{i,k+1} = \hat{z}^+_{i,k} \quad \forall i \in \{1, \ldots, N\} \tag{31}$$

where $\hat{f}_k = \tilde{f} - \hat{b}_{f,k}$ and $\hat{\omega}_k = \tilde{\omega} - \hat{b}_{\omega,k}$ denote the expected values of the measured acceleration and angular velocity, respectively. Note that the quaternion representing the base pose is updated using the exponential map formed from the infinitesimal IMU rotation $\omega \Delta t$ which is measured in the base frame directly. Also note that a second-order discretization is used for the position in order to incorporate the IMU acceleration.

The measurement model is discretized simply as

$$\hat{s}_{p,k} = \hat{C}^-_k(\hat{p}^-_k - \hat{r}_k) \tag{32}$$

$$\hat{s}_{z,k} = \hat{q}^-_k \otimes \left(\hat{z}^-_k\right)^{-1} \tag{33}$$

to produce the expected measurement of the nonlinear system as in (4).

B. Continuous, Linear Model

Recall that linearized dynamics are required in order to propagate the state estimate covariance and perform the EKF update step. However, we also need to discretize these linearized dynamics in order to implement the discrete EKF. As a matter of preference, we choose to linearize and then discretize; this is the approach found in many texts.

Linearization is performed by expanding each state in the prediction model around its current estimate using a first-order Taylor series approximation.[1]

This approach results in the linearized model

[1]For the full derivation of the linearized system presented in this section, see http://www-clmc.usc.edu/∼nrotella/Sites/IROS_linearization.pdf (to be updated in the event of publication)

$$\dot{\delta r} = v \tag{34}$$
$$\dot{\delta v} = -C^T f^\times \delta\phi - C^T \delta b_f - C^T w_f \tag{35}$$
$$\dot{\delta\phi} = -\omega^\times \delta\phi - \delta b_\omega - w_\omega \tag{36}$$
$$\dot{\delta p} = C^T w_p \tag{37}$$
$$\dot{\delta b_f} = w_{bf} \tag{38}$$
$$\dot{\delta b_\omega} = w_{b\omega} \tag{39}$$
$$\dot{\delta\theta} = w_z \tag{40}$$

where the measured IMU quantities are bias-compensated and where $v^\times$ denotes the skew-symmetric matrix corresponding to the vector v. The error state vector and the process noise vector are defined to be $\delta x = [\delta r, \delta v, \delta\phi, \delta p, \delta b_f, \delta b_\omega, \delta\theta]^T$ and $w = [w_f, w_\omega, w_p, w_{bf}, w_{b\omega}, w_z]^T$, respectively. The linearized system can then be written in state-space form as $\dot{\delta x} = F_c \delta x + L_c w$ where

$$F_c = \begin{pmatrix} 0 & I & 0 & 0 & 0 & 0 & 0 \\ 0 & 0 & -C^T f^\times & 0 & -C^T & 0 & 0 \\ 0 & 0 & -\omega^\times & 0 & 0 & -I & 0 \\ 0 & 0 & 0 & 0 & 0 & 0 & 0 \\ 0 & 0 & 0 & 0 & 0 & 0 & 0 \\ 0 & 0 & 0 & 0 & 0 & 0 & 0 \\ 0 & 0 & 0 & 0 & 0 & 0 & 0 \end{pmatrix}$$

is the prediction Jacobian defined by (5) and the noise Jacobian L_c does not appear in the EKF formulation. It is assumed for simplicity that the covariance matrix of each process noise vector is diagonal with equal entries. The continuous process noise covariance matrix is then

$$Q_c = E[ww^T] = diag\{Q_f, Q_\omega, Q_p, Q_{b_f}, Q_{b_\omega}, Q_z\}$$

The measurement model defined by (23) and (24) is linearized as

$$s_p = -C\delta r + C\delta p + (C(p-r))^x \delta\phi + n_p$$
$$s_z = \delta\phi - C[z \otimes q^{-1}]\delta\theta + n_z$$

where $C[m]$ is used to denote the rotation matrix corresponding to the quaternion m. This model can be written in the form $z = H_c \delta x + v$ where $v = [n_p, n_z]^T$ is the measurement noise vector and

$$H_c = \begin{pmatrix} -C & 0 & (C(p-r))^x & C & 0 & 0 & 0 \\ 0 & 0 & I & 0 & 0 & 0 & -C[z \otimes q^{-1}] \end{pmatrix}$$

is the measurement Jacobian as defined by (6). It is assumed that measurements are uncorrelated and hence the measurement noise covariance matrix is defined as $R_c = diag\{R_p, R_z\}$ where R_p and R_z are again each diagonal with equal entries.

C. Discrete, Linear Model

Assuming a zero-order hold over the interval $\Delta t = t_{k+1} - t_k$, the discretized process Jacobian is given by

$$F_k = e^{F_c \Delta t}$$

and the discretized state covariance matrix is given by

$$Q_{k-1} = \int_{t_{k-1}}^{t_k} e^{F_c(t_k - \tau)} L_c Q_c L_c^T e^{F_c^T (t_k - \tau)} d\tau$$

These are standard results detailed in many texts on state-space controls. In practice, the series which define the discrete dynamics matrix and state covariance matrix are often truncated at first order for simplicity to yield $F_{k-1} \approx I + F_c \Delta t$ and $Q_{k-1} \approx Q_c \Delta t$. In contrast to [1], such a first-order discretization is employed in order to simplify the implementation. It was observed that these approximations did not affect filter performance in any significant way.

Following the above procedure, we find the discretized dynamics and process noise covariance matrices to be

$$F_k = \begin{pmatrix} I & I\Delta t & 0 & 0 & 0 & 0 & 0 \\ 0 & I & -C_k^T f_k^\times \Delta t & 0 & -C_k^T \Delta t & 0 & 0 \\ 0 & 0 & I - \omega_k^\times \Delta t & 0 & 0 & -I\Delta t & 0 \\ 0 & 0 & 0 & I & 0 & 0 & 0 \\ 0 & 0 & 0 & 0 & I & 0 & 0 \\ 0 & 0 & 0 & 0 & 0 & I & 0 \\ 0 & 0 & 0 & 0 & 0 & 0 & I \end{pmatrix},$$

$$Q_k = diag\{\Delta t Q_f, \Delta t Q_\omega, \Delta t Q_p, \Delta t Q_{b_f}, \Delta t Q_{b_\omega}, \Delta t Q_z\}$$

where all quantities are computed using the *a priori* state vector $\hat{x}_k^-$. The discrete measurement Jacobian is simply

$$H_k = \begin{pmatrix} -C_k & 0 & (C_k(p_k - r_k))^\times & C_k & 0 & 0 & 0 \\ 0 & 0 & I & 0 & 0 & 0 & -C[z_k \otimes_k^{-1}] \end{pmatrix}$$

Finally, the continuous measurement covariance matrix is discretized as $R_{k-1} \approx \frac{R_c}{\Delta t}$.

D. Observability Analysis

As in [1], a nonlinear observability analysis of the filter was performed. This section discusses the resulting observability characteristics of the proposed approach and analyzes the theoretical advantages of the addition of the foot pose constraint. Briefly, analyzing the observability of a nonlinear system involves computing gradients of Lie derivatives of the measurement model (2) with respect to the process model (1) as presented in [12]. While the full derivation is omitted for brevity, the pertinent results are summarized in tables I, II, and III below.[2]

The unobservable subspace - which, informally, describes all directions along which disturbances cannot be observed at

[2]For the full derivation of the observability analysis presented in this section, see http://www-clmc.usc.edu/∼nrotella/Sites/IROS_observability.pdf (to be updated in the event of publication)

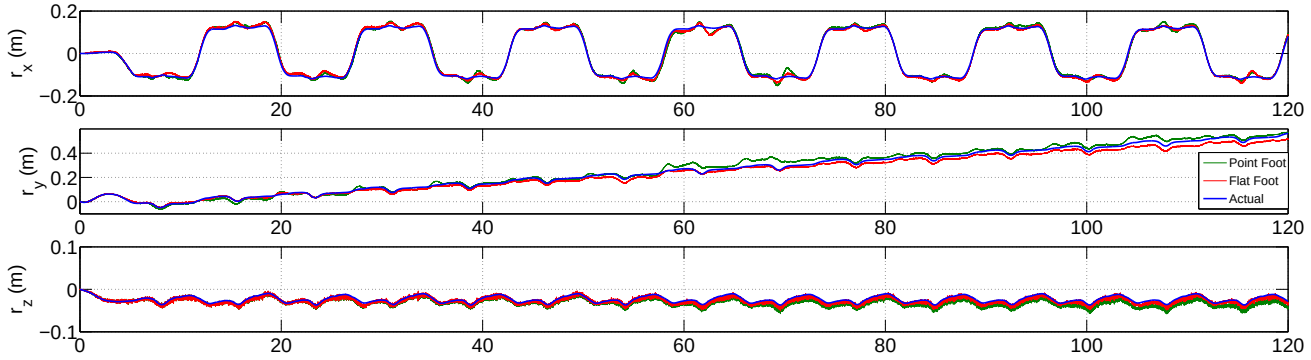

(a) Position

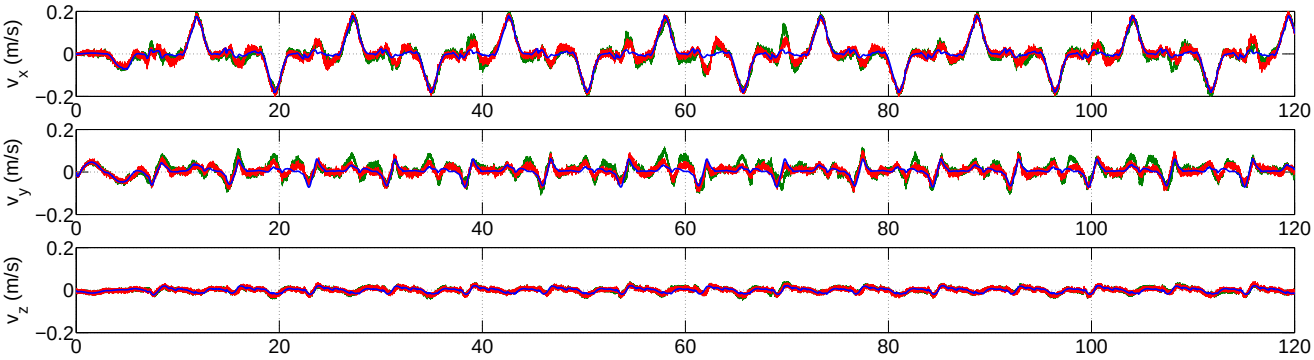

(b) Velocity

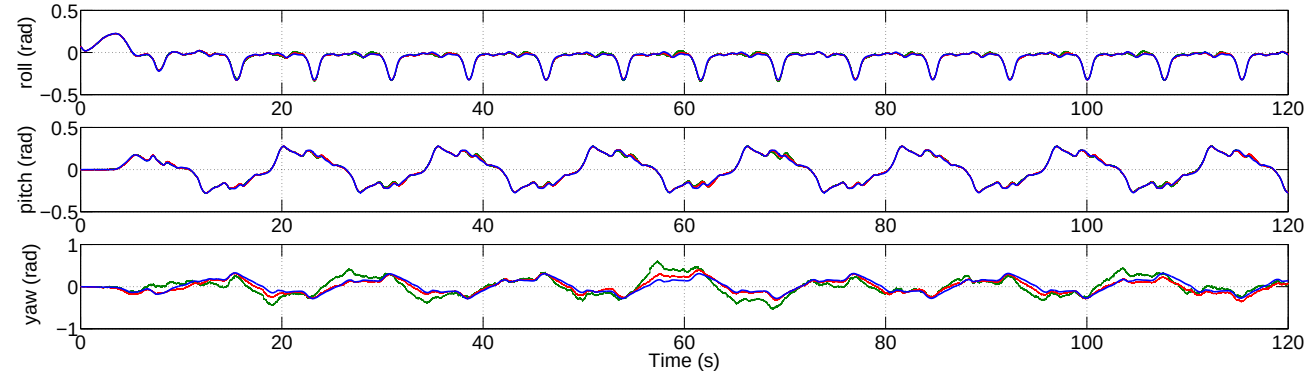

(c) Euler Angles

Fig. 1: Position, velocity and orientation (Euler angle) estimates for the 120 second walking task. Note that the divergence in the position and yaw angle are to be expected as these states are always unobservable. Overall, the flat foot filter introduced in this work performs noticeably better than the filter introduced in [1] as confirmed by the RMS tracking errors listed in Table IV.

the system output - can change depending on the motion of the system. The presented analysis is extensive and reveals all possible singularities and corresponding rank losses (RL). Note that since the absolute position and yaw angle are inherently unobservable in the presented system, rank loss as described below represents an increase in the dimension of the unobservable subspace beyond this nominal case.

Table I describes the rank deficiency for the case in which a single point foot is in contact with the ground. The rows of this table can be interpreted as follows. The top row ($w = 0$) describes the case in which there is no rotational motion. Depending on the acceleration, the rank loss is either 3 or 5. The second row ($w \perp Cg$) states that whenever there is rotational motion around an axis which is perpendicular to the gravity axis then the rank loss is 1 (interestingly, this singularity arises within all other scenarios as well). The third row ($w \parallel Cg$) describes the slightly more complicated case in which there is a rotation around the gravity axis only; in general, this corresponds to a rank loss of 1. In the subcase in which the axis of rotation intersects the point of contact, rank loss increases to 2. If in addition the IMU is directly above the point of contact, the rank loss further increases to 3. Finally, the last row states that if the rotational motion is neither aligned with the gravity axis nor perpendicular to it then the system does not exhibit any rank deficiency beyond the nominal case.

Rotation	Acceleration/Velocity	Foothold	RL
$w = 0$	$a = -1/2g$	$*$	5
	$a \neq -1/2g$	$*$	3
$w \perp Cg$	$*$	$*$	1
$w \parallel Cg$	$\wedge \begin{array}{l} a = \left(C^T w\right) \times v \\ v = \left(C^T w\right) \times (r-p) \end{array}$	$(r-p) \parallel g$	3
		$(r-p) \not\parallel g$	2
	$\vee \begin{array}{l} a \neq \left(C^T w\right) \times v \\ v \neq \left(C^T w\right) \times (r-p) \end{array}$	$*$	1
$\wedge \begin{array}{l} w \not\perp Cg \\ w \not\parallel Cg \end{array}$	$*$	$*$	0

TABLE I: Rank deficiency for a single point foot contact.

The following table summarizes the rank-deficient cases for two point foot contacts. The singular cases are similar to those for a single point contact but with reduced rank losses.

Rotation	Footholds	RL
$w = 0$	$2a + g \parallel \Delta p$	3
	$2a + g \not\parallel \Delta p$	2
$w \perp Cg$	$*$	1
$w \parallel Cg$	$g \parallel \Delta p$	1
	$g \not\parallel \Delta p$	0
$\wedge \begin{array}{l} w \not\perp Cg \\ w \not\parallel Cg \end{array}$	$*$	0

TABLE II: Rank deficiency for two point foot contacts.

In comparison to the point foot case, the observability analysis for the flat foot case is significantly simpler to compute and interpret. The following table summarizes the results for this case. Note that these results are valid for an arbitrary number of flat foot contacts; informally, this means that additional contacts beyond the first provide no new information. This makes sense since a single flat foot contact fully constrains the pose of the base.

Rotation	RL
$w = 0$	2
$w \perp Cg$	1
$w \not\perp Cg$	0

TABLE III: Rank deficiency for an arbitrary number of flat foot contacts.

Table III shows that the rank loss for the new filter depends only on the angular velocity. If the angular velocity is zero then the rank loss is 2; if the axis of rotation is perpendicular to the gravity axis then the rank loss is 1. For all other cases the rank loss is 0; only the absolute position and yaw angle are unobservable.

It's clear that the additional information resulting from the the rotational constraint of the foot significantly reduces rank loss, as expected. In summary, the maximum rank loss is reduced from 5 to 2 when there is no rotational motion. Additionally, rotation purely around the gravity axis no longer induces rank loss. The results of section VII reinforce the above analysis and demonstrate the practical effects of the singular cases.

VI. Experimental Setup

The end goal of this work is to implement the proposed EKF on a SARCOS humanoid robot equipped with a Microstrain 3DM-GX3-25 IMU in order to provide robust state estimation for legged locomotion tasks. Before testing the filter on the humanoid, however, it was desired that its performance be verified in simulation. For this purpose, both the original filter proposed in [1] and the new filter were implemented in the SL simulation environment [13] according to the theory described in previous sections. In order to ensure a smooth transition to the actual robot as well as to provide an accurate assessment of the approach, process and measurement noise models were developed and realistic levels of noise were added in the simulator.

The IMU model detailed in [1] assumed that inertial data from both the accelerometer and gyroscope are afflicted by a combination of thermal noise and drift (bias). Thermal noise was added to the simulated sensor data by drawing samples from an independent and identically-distributed Gaussian white noise process parameterized by its variance. Sensor bias, which is modeled as the integral of white noise, was stored for each sensor and updated at every timestep using a first-order integration scheme before being added to the simulated data. Similarly, measurement noise was added to the relative position and orientation measurements at each timestep by drawing samples from a white noise process parameterized by measurement noise variances.

The standard deviations of the additive Gaussian white noise processes for the accelerometer (w_f) and gyroscope (w_ω) were fixed at $0.00078 m/s^2/\sqrt{Hz}$ and $0.000523 rad/s/\sqrt{Hz}$ respectively; the standard deviations of the bias white noise processes for the accelerometer

(w_{bf}) and gyroscope ($w_{b\omega}$) were fixed at $0.0001m/s^3/\sqrt{Hz}$ and $0.000618rad/s^2/\sqrt{Hz}$ respectively. These values were derived from specifications given on the 3DM-GX3-25 datasheet. Note that these noise parameters are converted to discrete variances by squaring them and dividing by the timestep. The noise on the relative position (n_p) and orientation (n_z) measurements were defined directly in the discrete domain to have standard deviations of $0.01m$ and $0.01rad$, respectively. These values were chosen based on the observed uncertainty in the encoders and kinematic model of the actual robot. All experiments were conducted at an update rate of 1000Hz as this is the control frequency used on the SARCOS platform (as well as the fastest rate at which raw acceleration and angular velocity signals can be streamed from the IMU).

The standard deviations of the foot position (w_p) and orientation (w_z) noise were set to $0.001m/\sqrt{Hz}$ and $0.001rad/\sqrt{Hz}$ respectively, allowing for a small amount of slippage in both position and orientation at the contacts. Note that on the real robot these foothold noise parameters would normally be tuned in different directions based on the characteristics of expected contacts. Further, the measurement noise parameters would be tuned in order to compensate for inaccuracies and assumptions in the model. We chose to use exact knowledge of the simulated noise in experiments in order to focus on the theoretical characteristics of the presented filter. Initialization of the base orientation was performed using accelerometer measurements, initial foot poses were computed from kinematics and all other states were initialized to zero.

VII. Results and Analysis

The plots in Figure 1 show the results obtained on the simulated walking dataset of length 120 seconds. In addition, Table IV lists the RMS errors for all plotted quantities (where the last three rows correspond to the Euler angles roll, pitch and yaw). Note that while both filters perform well, the flat foot filter has lower RMS errors than the point foot filter for all quantities plotted. This is to be expected, as the additional measurements incorporated in the flat foot filter constrain the rotational states. Additionally, the rank loss cases for the flat foot filter are fewer and less drastic, meaning that as the robot moves through a complex task it is less likely to encounter these cases.

A second experiment was performed on a simulated squatting dataset in which the robot performed squats at $1Hz$ for 120 seconds, attaining velocities as high as $0.3m/s$. This task is meant to demonstrate that the filter can handle more rapid motion as well as sustained motion over a long period of time. The results are not plotted for the sake of brevity but the RMS error values are again given in Table IV.

	Walking		Squatting	
	Point Foot	Flat Foot	Point Foot	Flat Foot
$r_x(m)$	0.0099	0.0077	0.0052	0.0035
$r_y(m)$	0.0221	0.0211	0.0015	0.0013
$r_z(m)$	0.0088	0.0042	0.0017	0.0018
$v_x(m/s)$	0.0212	0.0175	0.0121	0.0093
$v_y(m/s)$	0.0249	0.0141	0.0074	0.0066
$v_z(m/s)$	0.0074	0.0065	0.0048	0.0044
$\alpha(rad)$	0.0108	0.0107	0.0027	0.0018
$\beta(rad)$	0.0074	0.0053	0.0052	0.0034
$\gamma(rad)$	0.1371	0.0517	0.0386	0.0227

TABLE IV: RMS error values for the 120 second walking and squatting tasks.

VIII. Conclusions

This paper introduces an EKF for state estimation on humanoid robots which builds on the filter introduced in [1]. These extensions to the previous work are shown to improve the observability characteristics of the system as well as improve performance on a realistic simulated platform. In future work, the filter will be implemented and verified on the SARCOS robot through extensive testing in balancing and locomotion tasks. Additional extensions to the presented framework involving new sensors will be investigated and the resulting formulations will be compared against the filter presented here.

References

[1] M. Bloesch, M. Hutter, M. Hoepflinger, S. Leutenegger, C. Gehring, C. D. Remy, and R. Siegwart, "State estimation for legged robots - consistent fusion of leg kinematics and IMU," in *Proceedings of Robotics: Science and Systems*, Sydney, Australia, July 2012.

[2] G. P. Roston and E. Krotkov, "Dead reckoning navigation for walking robots," Robotics Institute, Pittsburgh, PA, Tech. Rep. CMU-RI-TR-91-27, November 1991.

[3] B. Gassmann, F. Zacharias, J. Zollner, and R. Dillmann, "Localization of walking robots," in *Robotics and Automation, 2005. ICRA 2005. Proceedings of the 2005 IEEE International Conference on*, April 2005, pp. 1471–1476.

[4] P.-C. Lin, H. Komsuoglu, and D. Koditschek, "Sensor data fusion for body state estimation in a hexapod robot with dynamical gaits," *Robotics, IEEE Transactions on*, vol. 22, no. 5, pp. 932–943, Oct 2006.

[5] S. Chitta, P. Vernaza, R. Geykhman, and D. Lee, "Proprioceptive localilzatilon for a quadrupedal robot on known terrain," in *Robotics and Automation, 2007 IEEE International Conference on*, April 2007, pp. 4582–4587.

[6] J. A. Cobano, J. Estremera, and P. Gonzalez de Santos, "Location of legged robots in outdoor environments," *Robot. Auton. Syst.*, vol. 56, no. 9, pp. 751–761, Sept. 2008. [Online]. Available: http://dx.doi.org/10.1016/j.robot.2007.12.003

[7] M. Reinstein and M. Hoffmann, "Dead reckoning in a dynamic quadruped robot: Inertial navigation system aided by a legged odometer," in *Robotics and Automation (ICRA), 2011 IEEE International Conference on*, May 2011, pp. 617–624.

[8] A. Chilian, H. Hirschmuller, and M. Gorner, "Multisensor data fusion for robust pose estimation of a six-legged walking robot," in *Intelligent Robots and Systems (IROS), 2011 IEEE/RSJ International Conference on*, Sept 2011, pp. 2497–2504.

[9] S. Park, Y. Han, and H. Hahn, "Balance control of a biped robot using camera image of reference object," *International Journal of Control, Automation and Systems*, vol. 7, no. 1, pp. 75–84, 2009. [Online]. Available: http://dx.doi.org/10.1007/s12555-009-0110-2

[10] L. Wang, Z. Liu, C. Chen, Y. Zhang, S. Lee, and X. Chen, "A ukf-based predictable svr learning controller for biped walking," *Systems, Man, and Cybernetics: Systems, IEEE Transactions on*, vol. 43, no. 6, pp. 1440–1450, Nov 2013.

[11] N. Trawny and S. I. Roumeliotis, "Indirect Kalman filter for 3D attitude estimation," University of Minnesota, Dept. of Comp. Sci. & Eng., Tech. Rep. 2005-002, Mar. 2005.

[12] R. Hermann and A. J. Krener, "Nonlinear controllability and observability," *Automatic Control, IEEE Transactions on*, vol. 22, no. 5, pp. 728–740, Oct 1977.

[13] S. Schaal, "The sl simulation and real-time control software package," University of Southern California, Dept. of Comp. Sci., Tech. Rep., 2007.